Spectroscopic Techniques

Applied Spectroscopy

Applied Spectroscopy
2024, Vol. 78(10) 1098–1104

DOI: 10.1177/00037028241267892
journals.sagepub.com/home/asp
Sage

Feasibility of a Fiber-Dispersive Raman Spectrometer for Biomarker Detection

Mariia Sidorova[1,2], Sergey G. Pavlov[2], Ute Böttger[3], Mickael Baqué[3], Alexei D. Semenov[2], and Heinz-Wilhelm Hübers[1,2]

Abstract

Raman spectroscopy is among the top analytical techniques for ultra-low-dense organic matter, crucial to the search for life and analysis of celestial body surfaces in space exploration missions. Achieving the ultimate sensitivity of in-situ Raman spectroscopy necessitates a breakthrough in detecting inelastically scattered light. Single-photon detectors (SPDs) operating in photon counting mode, which can differentiate between Raman and luminescence responses, are promising candidates for the challenging scientific requirements. Since large SPD arrays are not yet commercially available, a dispersive element can be adapted to a single-pixel detector. By exploiting chromatic dispersion in optical fibers and picosecond-pulsed excitation, we delay the arrivals of different spectral components onto a single-pixel SPD. This method also separates weak Raman signals from stronger luminescence through correlated time-domain measurements. We study the impact of fiber properties and the excitation wavelength of a pulsed laser on the spectral resolution of the fiber-dispersive Raman spectrometer (FDRS). Additionally, we demonstrate the FDRS's potential for studying biomarkers and discuss its feasibility for analyzing inclusions in ice matrices.

Keywords

Fiber-dispersive Raman spectrometer, superconducting nanowire single-photon detector, biomarkers, ice matrices

Date received: 8 March 2024; accepted: 19 June 2024

Introduction

Raman spectroscopy is a powerful analytical technique for the detection and identification of low-dense biological matter in inorganic matrices, crucial for both terrestrial and extraterrestrial research. For instance, conventional confocal Raman systems have demonstrated their capability to identify mineral inclusions and organic matter in the water ice cores from a subglacial Antarctic lake.[1] Within the BIOMEX project, conventional Raman spectroscopy assessed the stability and degradation levels of space-exposed biomolecules, embedded in martian and lunar regolith analogs.[2,3] Despite their relatively large Raman cross sections, biomolecules are unlikely to be present on extraterrestrial surfaces at a density that ensures their reliable detection; only a few Raman scattered photons can be expected to be available under laser illumination with a spot diameter of 50–100 µm on regolith. Distinguishing a few Raman photons from a vast amount of luminescence is hardly possible using conventional approaches. Achieving ultimate sensitivity for Raman spectroscopy can principally allow single-cell detection[4] that requires, however, dedicated improvements in instrument components.

To date, several space Raman instruments have been developed and are on board the Mars 2020 (SuperCam[5]) and ExoMars missions to Mars (RLS[6]), and JAXA MMX mission to Phobos and Deimos (RAX[7]). These visible-light instruments were primarily designed to detect bio-geological signatures of extraterrestrial life replicated in geological fingerprints of the surface and subsurface regolith. The Raman spectrometer SHERLOC on board the Mars 2020 mission uses deep-ultraviolet excitation to enhance Raman intensities of organic molecules.[8] These instruments, relying on conventional Raman spectroscopy with a diffraction grating as a dispersive element and a multi-pixel detector array based on charge-coupled devices, face challenges in detecting low-

[1]Humboldt-Universität zu Berlin, Department of Physics, Berlin, Germany
[2]German Aerospace Center (DLR), Institute of Optical Sensor Systems, Berlin, Germany
[3]German Aerospace Center (DLR), Institute of Planetary Research, Berlin, Germany

Corresponding author:
Mariia Sidorova, Humboldt-Universität zu Berlin, Department of Physics, Newtonstrasse 15, 12489 Berlin, Germany.
Email: mariia.sidorova@dlr.de

dense biological matter. These challenges include requirements of non-destructive fluences of the used excitation lasers which implies low Raman intensities as well as the presence of a strong luminescence background.

A novel approach, combining pulsed laser excitation, a single-photon detector (SPD), and a fiber-dispersive element for Raman spectrometer (FDRS) can rise to these challenges.[9,10] The FDRS, utilizing SPD, promises a fundamentally lower detection limit and, additionally, may select the weak instantaneous pulsed Raman signal from often accompanying luminescence with lifetimes longer than the excitation pulse duration. This approach minimizes the risk of damaging biological samples and reduces the weight and power consumption of spaceborne instruments. The feasibility of lightweight FDRS for in-situ analysis on space missions, by incorporating semiconducting-based SPDs has been discussed elsewhere.[11]

It is commonly accepted that a spectral resolution of sub-10 cm^{-1} within the 100–4000 cm^{-1} Stokes-shift range is sufficient for accurate identification of both inorganic and organic matter. For conventional spectrometers, which use a diffraction grating to spatially disperse spectral components onto a multi-pixel detector, the resolution is essentially determined by the grating's groove density and the spectrometer's size. Conversely, the FDRS approach exploits a long dispersive fiber to delay the arrival of different spectral components onto a single-pixel SPD. The detector measures the arrival times, which are further correlated to the laser pulse via time-correlated single-photon counting (TCSPC) and translated into spectral data. Despite inherent limitations in temporal and spectral resolution, the FDRS approach meets the above-mentioned requirements for material identification (see analysis in Sidorova et al.[10]), achievable through the use of short (few ps), narrow-bandwidth (below 0.1 nm) laser pulses, long fibers (0.2–1 km of silica fiber), and an SPD with a high timing resolution (timing jitter, below 20 ps).

This study assesses the critical parameters of the FDRS components, in both time and frequency domains, controlling spectral resolution at different Stokes shifts. We demonstrate how laser excitation wavelength and fiber dispersion affect the spectral resolution of such a fiber-dispersive Raman approach. To expand the application scope of FDRS and illustrate its versatility in detecting diverse substances, we analyze key biomolecules and briefly discuss the advantages and challenges of using Raman spectroscopy for in situ analysis of inclusions in ice matrices.

Experimental

Fiber-Dispersive Raman Spectrometer (FDRS)

The principle of the FDRS is depicted in Figure 1. It retains several components of a conventional Raman spectrometer, such as an excitation laser and longpass (wavelength) filters to suppress the Rayleigh light, while introducing a novel dispersive element and detector. Exciting a sample with a short laser pulse, characterized by duration σ_{t0} and spectral bandwidth $\sigma_{\lambda 0}$, generates a short (in time), broadband (in frequency) pulsed Raman signal. The FDRS uses a long optical fiber for dispersion that delays the arrival of different spectral components at the detector, thereby converting spectral information into delay times. A low-jitter, single-pixel detector generates an electrical signal in response to each detected Raman photon. The TCSPC electronics then

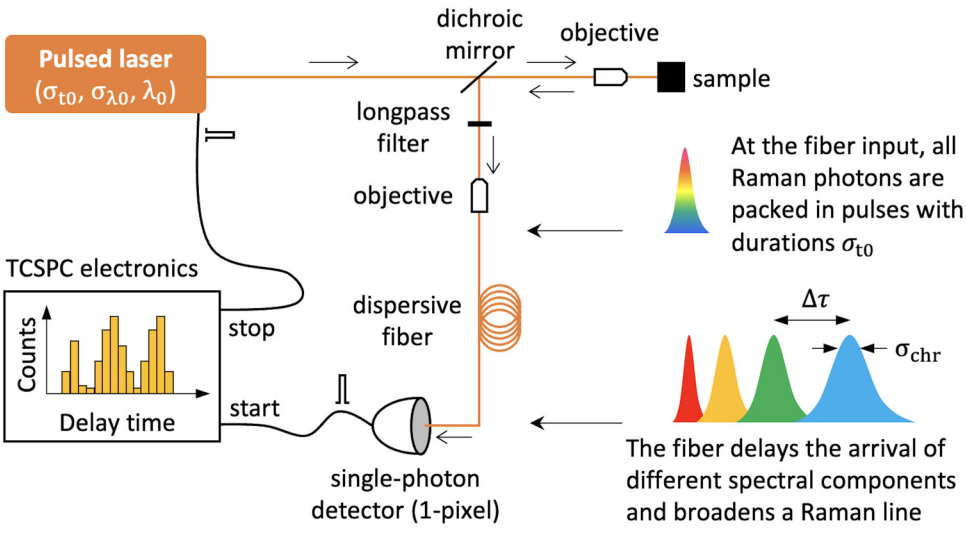

Figure 1. Key components and principle of the FDRS. Laser pulses at the sample, characterized by duration σ_{t0}, bandwidth $\sigma_{\lambda 0}$ (in standard deviation), and central wavelength λ_0, generate Raman scattered light as a broadband pulse. This pulse, when propagating through the dispersive fiber, experiences delays of its spectral components; $\Delta\tau$ denotes the delay in arrivals at the detector, and σ_{chr} is the broadening of a Raman line due to chromatic dispersion. TCSPC electronics correlates these delays to the laser reference, providing the Raman spectra in the time domain. Details are elaborated in the main text.

assigns delay times to these signals relative to the laser reference. To ensure accurate statistics of delay times, the entire range of time-dispersed Raman spectra (and luminescence, if any) must not exceed the laser pulse period.

Two pulses with central wavelengths λ_1 and λ_2 propagating through the fiber length L get delayed due to group velocity dispersion by the delay time $\Delta\tau = L\int_{\lambda_1}^{\lambda_2} D(\lambda)\, d\lambda$, where $D(\lambda)$ is the dispersion coefficient. Besides being delayed, the pulses also broaden in time due to chromatic dispersion with $\sigma_{chr} = L|D(\lambda)|\sigma_{\lambda 0}$ representing this broadening, where $\sigma_{\lambda 0}$ is the finite spectral bandwidth of a pulse. To reconstruct the spectral information from the time domain, one needs to know $\tau(\lambda)$, which can be either computed using the fiber's specifications or through calibration.

For proof-of-principle demonstration, we equipped our FDRS with a superconducting nanowire SPD (Scontel, control unit with amplifiers CU-2SPD/P&T-005), which showed 5 ns dead time and 26 ps timing jitter (in standard deviation), time-correlated electronics (Becker and Hickl, SPC-150NX), and two pulsed lasers: a picosecond 532 nm laser (PicoQuant, diode laser head LDH-P-FA-530B with driver PDL 800-D) with the pulse duration $\sigma_{t0} = 19$ ps and the bandwidth $\sigma_{\lambda 0} < 0.1$ nm (below 3.5 cm^{-1}) and a femtosecond 785 nm laser (Femtosource, synergy 20) with $\sigma_{t0} = 13$ fs and $\sigma_{\lambda 0} = 26$ nm (404 cm^{-1}), each operating at the repetition rate 80 MHz. A 45 m long graded-index fiber (Thorlabs, GIF50C), chosen for its reduced modal dispersion, which we disregard in our analysis, completes the FDRS's configuration. With the 785 nm laser, we incorporated a Raman probe (Ocean Optics, RPB785) comprising two step-index multimode fibers (each 1.5 m long, with a numerical aperture of 0.22, and core diameters of 105 µm and 200 µm) and optical filters, which are not depicted in Figure 1. Complementary measurements revealed these fibers contribute 18.5 ps/m pulse broadening and, together with filters, modify the 785 nm pulses at the sample to the duration 28 ps and the bandwidth 5 nm (77 cm^{-1}).

The FDRS was calibrated using methanol (CH_3OH) with characteristic Raman-active vibrational modes: 1030 cm^{-1} C–O stretching (str), 1450 cm^{-1} CH_3 antisymmetric deformation (def), 2840 and 2950 cm^{-1} CH_3 symmetric (s-str) and asymmetric stretching (d-str), respectively. Figures 2a and 2b show Raman spectra of CH_3OH in the time domain for the excitation wavelength $\lambda_0 = 532$ and 785 nm, respectively. A shorter λ_0 results in larger delays between given Raman modes and, therefore, provides a higher resolution. The resolved Raman peaks of CH_3OH are plotted in Figure 2c together with a calibration curve $\Delta\tau(\lambda)$, a fit to these peaks. We set the arrival of the zero-dispersion wavelength $\lambda_{ZD} \approx 1300$ nm to zero, at this wavelength $D(\lambda_{ZD}) = 0$.

The spectral resolution of the FDRS is defined as

$$\delta\lambda = \left(\sigma_{\lambda 0}^2 + \left(\frac{\sigma_\tau}{|d\tau/d\lambda|}\right)^2\right)^{1/2} \quad (1)$$

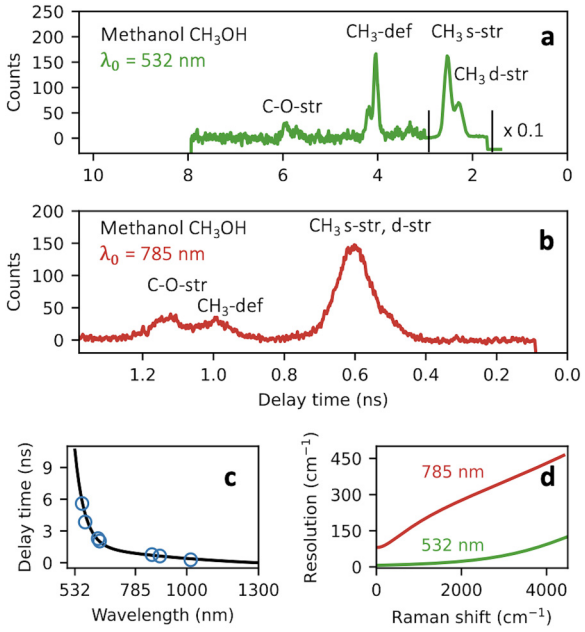

Figure 2. Fiber-dispersive Raman spectrometer (FDRS) calibration: time domain Raman spectra of CH_3OH was acquired with two pulsed lasers at (a) $\lambda_0 = 532$ nm and (b) $\lambda_0 = 785$ nm. The acquisition time and the bin size were 739 s and 3.05 ps for the spectrum shown in (a), and 628 s and 0.68 ps for (b). (c) Calibration curve for 45 m long dispersive fiber; symbols: marked Raman peaks of CH_3OH spectra. The arrival of λ_{ZD} is set to zero. (d) Spectral resolution of the FDRS with a 45 m long dispersive fiber and two excitation wavelengths computed with Eq. 1.

where the total pulse broadening σ_τ is given by

$$\sigma_\tau = \left(\sigma_{SPD}^2 + \sigma_{t0}^2 + \left(\sum_{j=1}^{n} \sigma_{chr,j}\right)^2 + \sum_{j=1}^{n} \sigma_{mod,j}^2 + \cdots\right)^{1/2} \quad (2)$$

This broadening accounts for the SPD timing resolution (jitter) σ_{SPD}, the excitation pulse duration, and the broadening due to chromatic (σ_{chr}) dispersion added by each of the n fiber segment with its particular length and core diameter, and other mechanisms such as modal dispersion (σ_{mod}), if present.[12] We found that the modal dispersion scales slower with the fiber length when it consists of several segments rather than one complete.[1]

By directly coupling laser pulses into the dispersive fiber, we measured the total broadening $\sigma_\tau$to be 40 and 145 ps at the 532 and 785 nm wavelengths, respectively, which sets an upper limit for our setup performance (8 cm^{-1} and 81 cm^{-1}, respectively). It is crucial to recognize that such significant broadening is due to non-optimized components of our spectrometer. Specifically, at 785 nm, the main limiting factors are the wide spectral bandwidth (77 cm^{-1}) and long duration (28 ps) of the excitation pulses (after passing through additional optical components as discussed above),

while, at 532 nm, the resolution is constrained by the long pulse duration (19 ps) combined with substantial SPD jitter (26 ps).

We then compute the resolution in wavelength using Eq. 1 and convert it into wavenumbers as $\delta\nu = (\lambda^{-1} - (\lambda + \delta\lambda)^{-1}) \times 10^7$. This computed resolution is plotted in Figure 2d as a function of Raman wavenumber shift $(\lambda_0^{-1} - \lambda^{-1}) \times 10^7$. We emphasize that the current resolution, although limited by the non-optimized FDRS components discussed above, holds the potential for significant enhancement. Through dedicated selection and optimization of FDRS components, resolution below sub-5 cm^{-1} is achievable (see discussions around Figure 4 in Sidorova et al.[10]).

Fiber-Dispersive Raman Spectrometer (FDRS) Spectra of Organic Samples

After calibrating the FDRS, we performed time-domain Raman measurements on two organic samples: palmitic acid (CH_3–$(CH_2)_{14}$–COOH) and β-carotene ($C_{40}H_{56}$).

Figures 3a and 3b show the FDRS spectra of palmitic acid obtained with a 45 m long dispersive fiber, and lasers at wavelengths of 785 and 532 nm, respectively. Palmitic acid has characteristic Raman vibrational modes between 1400 and 1500^{-1} due to CH_2 or CH_3 deformations and in the 2840–2940 cm^{-1} range due to C–H stretching.[13,14] Notably, excitation with a shorter wavelength not only increases delays by a factor of four but also enhances the resolution. We refrain from making quantitative comparisons of resolution here due to the strong effect of the excitation pulses bandwidth ($\sigma_{\lambda 0} = 0.03$ and 5 nm for the 532 and 785 nm lasers, respectively) and modal dispersion introduced by additional multimode, step-index fibers (about 60 ps for the spectrum obtained with the 785 nm laser, not depicted in setup).

It is important to note that the superconducting detector used has a very broad single-photon sensitivity from the ultraviolet to the middle infrared range. The detector is integrated into an optical cavity that maximizes light absorption at 1550 nm wavelength. Although the exact structure of the cavity, and thus the detector's spectral sensitivity, remains unspecified, we speculate that it may exhibit a broad absorption peak at 1550 nm, a sensitivity dip around 800 nm, and absorption resonances peaks at shorter wavelengths around 320 and 530 nm.[15] Such characteristics are typical for optical cavities of commercial superconducting detectors and might elucidate the observed amplitude variations in the detected Raman lines. Due to limited information on the spectral sensitivity of the detector used, we leave the quantitative analysis of the amplitudes of resolved Raman lines outside the scope of this work.

Figures 4a and 4b show FDRS spectra of β-carotene acquired with the 785 nm laser, and dispersive fiber with length 45 m and 90 m (two fibers of 45 m each were connected), respectively. β-carotene has two characteristic Raman modes around 1150 cm^{-1} and 1530 cm^{-1} due to C–C and C=C stretching, respectively. It is clear that doubling the fiber length results in as twice as long delays, it also improves the resolution by approximately 1.5 times (the widths of resolved C=C Raman modes are 150 and 100 cm^{-1} obtained with the 45 m and 90 m long fibers, respectively).

It is worth noting that increasing the length of the dispersive fiber causes two effects with opposite impacts on the spectral resolution: (i) increase in the delay between given

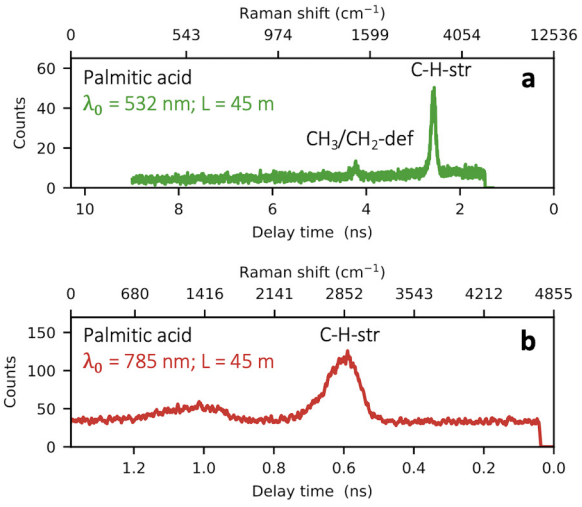

Figure 3. Time-domain FDRS Raman spectra of palmitic acid, obtained using 45 m long dispersive fiber and pulsed lasers at wavelengths of (a) $\lambda_0 = 532$ nm and (b) $\lambda_0 = 785$ nm. The arrival time of the zero-dispersion wavelength λ_{ZD} is set to zero. The acquisition time and the bin size were 399 s and 2.04 ps for the spectrum shown in (a), and 496 s and 0.68 ps for (b).

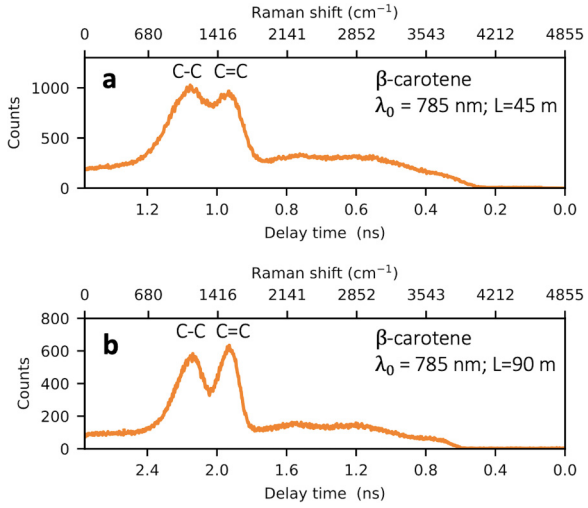

Figure 4. Time-domain FDRS Raman spectra of β-carotene, obtained using a pulsed laser at $\lambda_0 = 785$ nm and a dispersive fiber with the length (a) $L = 45$ m and (b) $L = 90$ m. The arrival of λ_{ZD} wavelength is set to zero. The acquisition time and the bin size were 88 s and 0.68 ps for the spectrum shown in (a), and 50 s and 1.02 ps for (b).

spectral components which improves the resolution (the second term in Eq. 1 decreases as $|d\tau/d\lambda|^{-1} \propto 1/L$), and (ii) increase in the pulse broadening due to chromatic dispersion (as well as modal dispersion, which is always present although might not be dominant) and worsens the resolution.

Results and Discussion

We would like to discuss the critical parameters of the FDRS elements in the context of space missions. Clearly, both approaches tested in this study, reducing the excitation wavelength and increasing the fiber length, improve the spectral resolution. Essentially, they both effectively enhance the dispersion. Thus, a straightforward strategy to improve spectral resolution would be to use dispersion-enhanced fibers such as, e.g., photonic crystal fibers. Their waveguide properties are determined by the arrangement of tiny air holes in glass, which run along the entire length of the fiber.[16] These fibers can be engineered to exhibit anomalously high dispersion,[17,18] increasing the resolution without extending the fiber length. While enhanced dispersion can lead to broadening, this can be mitigated by using narrow-bandwidth excitation pulses. The pulse bandwidth itself, however, does not determine the resolution limit of the spectrometer, as it is coupled to the pulse duration via the time-energy uncertainty principle as $\sigma_{\lambda 0} \propto \sigma_{t0}^{-1}$; the optimum combination $\sigma_{\lambda 0} = 0.05$ nm and $\sigma_{t0} = 3$ ps was found in Sidorova et al.[10] Alternatively, one can use single-mode fibers, which are completely free of undesired modal dispersion. Although chromatic dispersion in such fibers is usually weaker which requires longer fibers, it does not add much weight to the instrument (1 km of a silica fiber with a cladding diameter of 125 μm weighs about 30 g). Spectral resolution can be further improved via deconvolution of acquired Raman spectrum in the time domain, the procedure should account for both, the dispersion and the SPD's instrument response function (jitter). For instance, in superconducting nanowire SPDs used, the latter is described with an exponentially modified Gaussian distribution.[19]

Another critical FDRS's parameter is the timing resolution (jitter) of an SPD. Currently, superconducting nanowire-based SPDs offer the best timing performance and lowest noise but require cryogenic cooling that significantly increases the instrument's weight and limits their implementation in space missions.[20] In the visible range, a good alternative capable of single-photon counting with high timing resolution are semiconducting avalanche photodiodes and microchannel plate photomultiplier tubes, both can be implemented in a compact instrument.

Photon number resolution (PNR) can cause drawbacks, for instance, if TCSPC electronics is not capable of discriminating responses to individual photons. In a specific case of superconducting PNR detectors (e.g., Los et al.[21]), a Raman spectral line would be broadened to about 150 ps, the difference in delay times between electrical pulses generated in response to single-photon and multi-photon events. In this scenario, multi-photon detection occurs only if the photons' interarrival time is within a few picoseconds, a time dictated by intrinsic detection dynamics. At longer interarrival times, not exceeding the detector's dead time (about 5–20 ns), secondary photons are simply not detected.

One of the main advantages of the FDRS is its ability to suppress undesired luminescence through two inherent mechanisms. First, it uses picosecond excitation pulses, much shorter than the typical luminescence lifetimes (nanoseconds to sub-milliseconds), ensuring each luminescent compound is excited at most once per pulse, thus preventing luminescence from reaching its steady-state intensity. This mechanism is effective for luminescence that does not saturate at given optical pumping rates and has been demonstrated using a conventional charge-coupled device detector.[10] The second mechanism is akin to time-gating detection. It occurs when the Raman photons, dispersed over time, reach the detector before the slowly decaying luminescence photons, allowing their separation in the time domain when the luminescence lifetime exceeds the time-dispersed Raman spectra range (nanoseconds to microseconds, depending on the fiber length and dispersion). For this, pulsed lasers with adjustable repetition rates are most suitable to ensure the laser pulse period exceeds the luminescence decay time, avoiding signal overlap. It is worth noting that while these mechanisms effectively suppress luminescence, they do not eliminate it; luminescence and Raman photons generated within the duration of the excitation pulse remain indistinguishable.

Furthermore, since the FDRS exploits only a single-pixel detector, it is free from the noise caused by variations in pixel-to-pixel sensitivity present in conventional spectrometers with multi-pixel detector arrays.

In-Depth Raman Spectroscopy in Ice Matrices. Let us consider specific icy environments, where other challenges for the biomarker search by FDRS may dominate. The analysis of ice matrices is crucial for future astrobiological missions aimed at exploring celestial bodies such as icy moons. For instance, most icy moons with a dilute atmosphere are assumed to be covered with material from outer space and from their interiors. The latter can be ejected from the subglacial ocean in the form of gaseous or liquid jets mixed with solid fractions,[22] such as eruptions observed on Enceladus.[23] Because ice is a diffusely scattering medium, the capabilities for depth profiling in ice matrices, which may encapsulate bio/geologic matter, are defined by its transparency. The absorption minimum of water ice is in the visible range,[24] consequently, an excitation laser with the wavelength between 380 and 550 nm would be suitable to cover the Stokes range up to 4000 cm^{-1}.

We carried out comparative measurements with a commercial 532 nm Raman microscope (WITec Alpha 300) on two types of ice matrices taken at a temperature of −20 °C. Figure 5a shows fast-formed ice (a freezing rate

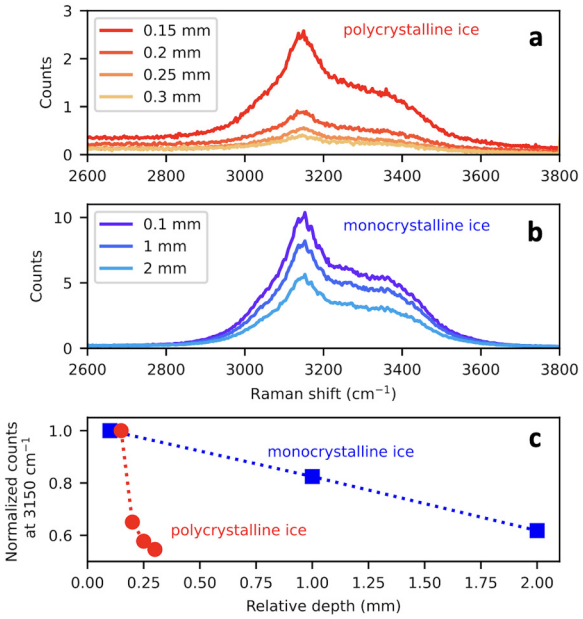

Figure 5. Spectra obtained with a commercial 532 nm Raman microscope of (a) polycrystalline and (b) accretion monocrystalline ice matrix from the subglacial Lake Vostok. Legends indicate different depths from the sample surface. (c) Decay of the Raman signal at 3150 cm^{-1} with the depth; symbols: experimental data, lines: guides to the eye.

of ≈1 mm per 10 min), created in the laboratory at 1 bar pressure to simulate the "surface" type environment of an icy moon. Figure 5b depicts slow-formed ice (at a rate of ≈3 m per year[25]) from the subglacial Antarctic lake Vostok (ice core from 3607 m depth). Both figures show a part of the Stokes range, characteristic of the OH vibrations of water ice. Strong diffusive scattering of light in the fast-formed ice, due to its polycrystalline structure and high defect density, causes a (quasi-) exponential decay in Raman signal-to-noise ratio (SNR) with depth, as seen in Figure 5c. In contrast, the accretion ice from Lake Vostok is monocrystalline and of high purity, showing a linear SNR decrease with depth, which facilitates in-depth exploration of potential organic inclusions.

It is important to note that when FDRS aims to probe deep into monocrystalline ice samples, photon migration time must be considered. This effect, due to the difference in propagation times of Raman photons from deeper molecules versus those closer to the ice surface, results in Raman line broadening. Specifically, probing into 10 mm depth would add ≈50 ps to the line broadening.

Conclusion

This study investigated the performance of the FDRS equipped with a single-pixel SPD for analyzing spectral responses from elementary biomolecules. Key findings include the impact of the laser wavelength and the fiber length. The visible picosecond 532 nm laser offers significantly better spectral resolution than the near-infrared femtosecond 785 nm laser, due to larger dispersion in the fiber material and reduced pulse broadening of spectrally narrower laser pulses. Doubling the fiber length improved spectral resolution by approximately 1.5 times. The FDRS offers the following advantages for astrobiological missions:

(i) Its inherent luminescence suppression capabilities combined with single-photon sensitivity enables the detection of low-density biologic matter at low excitation levels, minimizing the risk of sample deterioration. This is a significant improvement over current spaceborne Raman instruments, which struggle to differentiate a few Raman photons from the vast amount of luminescence.

(ii) Unlike conventional spectrometers, where high resolution over a wide spectral range is constrained by instrument size, the FDRS's spectral range is defined by the excitation and zero-dispersion wavelengths. It offers ultimate ranges of ≈ 5000 cm^{-1} and ≈ 12 500 cm^{-1} for silica fibers and the excitation 785 and 532 nm, respectively, and a sub-20 cm^{-1} resolution. Resolution can be further improved by extending the fiber length (enhancing the dispersion), which adds minimal weight to the instrument (<40 g/km of silica fiber).

(iii) The FDRS can be made compact by incorporating a lightweight detector with high timing resolution and single-photon sensitivity, such as visible-range avalanche photodiodes and photomultiplier tubes.

We note here that while stretching modes of biomolecules, C–C, C–H, C–O, etc., the spectral range of which is typically 1000–4000 cm^{-1}, provide the strongest Raman response and are the prime biosignatures. The differentiation between biomolecules very often requires the observation of usually weaker bending modes of internal bonds (a typical spectral range of 500–1600 cm^{-1}). Achieving the required resolution in the Stokes range may be possible with photonic crystal fibers or longer single-mode fibers.

Furthermore, operating Raman spectrometers with the capability for in-depth analysis is feasible. A combination of information on localization of the laser focus in the ice matrix together with the Raman signal-to-noise ratio using a confocal Raman microscope would return relevant complementary data on the structural properties of icy regolith.

Acknowledgments

The authors greatly acknowledge the support of S. A. Bulat for providing samples (the Vostok Lake accretion ice), David Vogt, Sven Frohman, and Enrico Dietz for technical assistance, and PicoQuant for the loan of laser head LDH-P-FA-530B and driver PDL 800-D.

Declaration of Conflicting Interests

The authors declared no potential conflicts of interest with respect to the research, authorship, and/or publication of this article.

Funding

The authors disclosed receipt of the following financial support for the research, authorship, and/or publication of this article: This study was supported by the Deutsches Forschungsgemeinschaft (DFG project No. 429811207).

ORCID iDs

Mariia Sidorova https://orcid.org/0000-0002-9082-442X
Sergey G. Pavlov https://orcid.org/0000-0002-7670-5694
Mickael Baqué https://orcid.org/0000-0002-6696-6030

Note

1. This result is based on empirical data from our previous research,[12] where we studied timing jitter of a superconducting detector and the broadening by chromatic and modal dispersion in fibers segments shorter than 20 m. Although we do not yet have an explanation for this effect, we speculate that it may arise due to intermodal coupling. This has been shown to slow down the broadening by modal dispersion with fiber length; from a linear law to the square root of fiber length (e.g., chapter "Fiber Optics" in Saleh and Teich[26]). However, this typically occurs in fibers much longer than those used in our studies.

References

1. U. Böttger, S. Bulat, F. Hanke, et al. "Identification of Inorganic and Organic Inclusions in the Subglacial Antarctic Lake Vostok Ice with Raman Spectroscopy". J. Raman Spectrosc. 2017. 48(11): 1503–1508.
2. J.P. de Vera, M. Alawi, T. Backhaus, et al. "Limits of Life and the Habitability of Mars: The ESA Space Experiment BIOMEX on the ISS". Astrobiology. 2019. 19(2): 145–157.
3. M. Baqué, T. Backhaus, J. Meeßen, et al. "Biosignature Stability in Space Enables Their Use for Life Detection on Mars". Sci. Adv. 2022. 8(36): eabn7412.
4. C. García-Timermans, R. Props, B. Zacchetti, et al. "Raman Spectroscopy-Based Measurements of Single-Cell Phenotypic Diversity in Microbial Populations". mSphere. 2020. 5(5): 30.
5. S. Maurice, R.C. Wiens, P. Bernardi, et al. "The SuperCam Instrument Suite on the Mars 2020 Rover: Science Objectives and Mast-Unit Description". Space Sci. Rev. 2021. 217(3): 1–108.
6. F. Rull, S. Maurice, I. Hutchinson, et al. "The Raman Laser Spectrometer for the ExoMars Rover Mission to Mars". Astrobiology. 2017. 17(6-7): 627–654.
7. Y. Cho, U. Böttger, F. Rull, et al. "In Situ Science on Phobos with the Raman Spectrometer for MMX (RAX): Preliminary Design and Feasibility of Raman Measurements". Earth Planets Space. 2021. 73(1): 1–11.
8. R. Bhartia, L.W. Beegle, L. DeFlores, et al. "Perseverance's Scanning Habitable Environments with Raman and Luminescence for Organics and Chemicals (SHERLOC) Investigation". Space Sci. Rev. 2021. 217(4): 1–115.
9. J. Toussaint, S. Dochow, I. Latka, et al. "Proof of Concept of Fiber Dispersed Raman Spectroscopy Using Superconducting Nanowire Single-Photon Detectors". Opt. Express. 2015. 23 (4): 5078–5090.
10. M. Sidorova, S. Pavlov, A. Semenov, et al. "Fiber-Dispersive Raman Spectrometer with Single-Photon Sensitivity". Opt. Express. 2021. 29(13): 20941–20951.
11. Z. Meng, G.I. Petrov, S. Cheng, et al. "Lightweight Raman Spectroscope Using Time-Correlated Photon-Counting Detection". Proc. Natl. Acad. Sci. U.S.A. 2015. 112(40): 12315–12320.
12. M. Sidorova, A. Semenov, A. Kuzmin, et al. "Intrinsic Jitter in Photon Detection by Straight Superconducting Nanowires". IEEE Trans. Appl. Supercond. 2018. 28(7): 1–4.
13. J. De Gelder, K. De Gussem, P. Vandenabeele, et al. "Reference Database of Raman Spectra of Biological Molecules". J. Raman Spectrosc. 2007. 38(9): 1133–1147.
14. K. Czamara, K. Majzner, M.Z. Pacia, et al. "Raman Spectroscopy of Lipids: A Review". J. Raman Spectrosc. 2015. 46(1): 4–20.
15. A.N. Vetlugin, F. Martinelli, S. Dong, et al. "Photon Number Resolution Without Optical Mode Multiplication". Nanophotonics. 2023. 12(3): 505–519.
16. P. Russell. "Photonic Crystal Fibers". Science. 2003. 299(5605): 358–362.
17. J.C. Knight. "Photonic Crystal Fibres". Nature. 2003. 424 (6950): 847–851.
18. Y. Jiang, B. Howley, Z. Shi, et al. "Dispersion-Enhanced Photonic Crystal Fiber Array for a True Time-Delay Structured X-Band Phased Array Antenna". IEEE Photonics Technol. Lett. 2004. 17(1): 187–189.
19. M. Sidorova, A. Semenov, H.W. Hübers, et al. "Physical Mechanisms of Timing Jitter in Photon Detection by Current-Carrying Superconducting Nanowires". Phys. Rev. B. 2017. 96(18): 184504.
20. I. Esmaeil Zadeh, J.W. Los, R.B. Gourgues, et al. "Efficient Single-Photon Detection with 7.7 ps Time Resolution for Photon-Correlation Measurements". ACS Photonics. 2020. 7(7): 1780–1787.
21. J. Los, M. Sidorova, B. Lopez-Rodriguez, et al. "High-Performance Photon Number Resolving Detectors for 850–950 nm Wavelength Range". APL Photonics. 2024. 9(6): 066101.
22. E. Lesage, H. Massol, S.M. Howell, et al. "Simulation of Freezing Cryomagma Reservoirs in Viscoelastic Ice Shells". Planet. Sci. J. 2022. 3(7): 170.
23. E.S. Kite, A.M. Rubin. "Sustained Eruptions on Enceladus Explained by Turbulent Dissipation in Tiger Stripes". Proc. Natl. Acad. Sci. U.S.A. 2016. 113(15): 3972–3975.
24. S.G. Warren, R.E. Brandt, T.C. Grenfell. "Visible and Near-Ultraviolet Absorption Spectrum of Ice From Transmission of Solar Radiation Into Snow". Appl. Opt. 2006. 45(21): 5320–5334.
25. L.M. Parker, P.M. Ross, W.A. O'Connor, et al. "Predicting the Response of Molluscs to the Impact of Ocean Acidification". Biology. 2013. 2(2): 651–692.
26. B.E. Saleh, M.C. Teich. Fundamentals of Photonics. Hoboken, New Jersey: John Wiley and Sons, 2019.